On the mechanism of fatigue and dwell-fatigue crack initiation in Ti-6Al-4V

Cyril Lavogiez, Samuel Hémery, Patrick Villechaise

On the mechanism of fatigue and dwell-fatigue crack initiation in Ti-6Al-4V

Cyril Lavogiez[a], Samuel Hémery[a,*], Patrick Villechaise[a]

[a] Institut Pprime, CNRS-ENSMA, Université de Poitiers, UPR CNRS 3346, Physics and Mechanics of Materials Departement, ENSMA – Téléport 2, 1 avenue Clément Ader, BP 40109, 86961 Futuroscope Chasseneuil Cedex, France

[*] Corresponding author: samuel.hemery@ensma.fr

Abstract

In the present study, the mechanism of fatigue and dwell-fatigue crack initiation was investigated in Ti-6Al-4V with a bi-modal microstructure. While substantial dwell-fatigue life debit was evidenced, microstructural configurations associated with crack nucleation are similar and suggest a unique mechanism for fatigue and dwell-fatigue loadings. Pairs of α grains well oriented for basal slip and separated by a (0001) twist grain boundary were found to be critical configurations for crack initiation. Intense slip is localized at the boundary and precedes crack formation along this boundary. These findings offer a new understanding and improved crack initiation prediction insights.

Keywords

Titanium alloys; fatigue; slip; grain boundary; dwell-fatigue

Main body

Titanium alloys are widely employed for aerospace applications including gas turbine components owing to a combination of superior mechanical properties with a relative low density [1]. In-service conditions imply complex cyclic loadings that include a hold time at high stress. This hold period leads to a reduction in number of cycles to failure [2,3]. This phenomenon, which is referred to as "dwell effect", is a major industrial concern and has been an active research field for more than 40 years. The life debit resulting from the introduction of a load hold is accompanied by a transition from surface to subsurface crack initiation of the crack leading to failure [2–6].

Early characterizations of the crystallographic orientation of subsurface initiation facets formed during dwell-fatigue tests revealed that the c-axis of the α titanium lattice is nearly parallel to the loading direction [2,3]. Using electron back-scattered diffraction (EBSD) and electron channeling techniques, it was also evidenced that the facet plane is close to the basal plane [4–6]. As a consequence, the misorientation between the c-axis of initiation α grains and the loading direction (denoted as declination angle in the following) is lower than 15° [6]. Evans and Bache introduced a modified version of the Stroh model in order to include a preliminary slip activity [7]. In this model, basal slip in the initiation grain, which is poorly oriented for <a> slip, is triggered by the stress concentration due to a dislocation pile up in an adjacent soft grain. Crystal plasticity simulations were used to update this model [8] to account for load shedding from the soft grain on to the hard grain [9–11] which assists crack nucleation [12–14].

Further analyses revealed declination angles up to 45° in α grains where dwell-fatigue facet nucleation occurred [15–18]. Basal slip activity being reported to occur in the 15 ° - 45° range [19–22], it is not clear whether cracks nucleate in hard or soft grains. Interestingly, this orientation domain is the same as reported for surface crack initiation that occurs in the primary α phase during low cycle fatigue tests [23,19,24–26]. In particular, several authors have shown that low cycle fatigue crack nucleation proceeds along basal slip bands in α grains well-oriented for basal slip [19,26–30]. While dwell-fatigue and fatigue crack initiation mechanisms are often addressed as different topics, literature data suggests that it might be rightful to consider a common crack initiation mechanism. This is the main motivation for the investigation of the crack initiation mechanism in Ti-6Al-4V submitted to fatigue and dwell-fatigue loadings reported in the present article.

Ti-6Al-4V with a bi-modal microstructure was studied. The microstructure is composed of equiaxed α (α_p) grains and secondary α (α_s) lamellas embedded in a β phase matrix. The surface fraction of the equiaxed α phase is 36% and the mean diameter is about 13 μm. Load controlled fatigue and dwell-fatigue tests were carried out using an INSTRON 1362 testing machine with a 100 kN loadcell. The strain was continuously acquired using an extensometer. Prior to testing, the surface of specimens was polished finishing with a mixture of colloidal silica with a particle size of 0.04 μm with 10% of H_2O_2. Loading and unloading segments were performed in 1s. The load ratio was equal to 0.1. The peak stress was set to 90% of the 0.2% proof stress, which was determined using a tensile test with a strain rate equivalent to the 1 s loading ramp. The minimum load was held for 1 s and the maximum load was held for 1 s or 120 s in order to obtain fatigue or dwell-fatigue loading conditions. Three fatigue tests and three dwell-fatigue tests were carried out up to failure in order to assess the fatigue and dwell-fatigue lives as they usually exhibit a substantial scatter [31]. Cylindrical fatigue specimens with a diameter of 4.3 mm and a gauge length of 13 mm were used for that purpose. This specimen geometry is referred to as T1 in the following.

Additional tests on differing sample types were stopped before failure in order to study crack initiation sites. The features of surface crack initiation sites were investigated using a modified specimen geometry including flat surfaces such as required for EBSD analysis. Three 2.5 mm wide and 8 mm long flat areas were machined on the gauge length of cylindrical fatigue specimens with a 6 mm diameter and a 8 mm gauge length. The flats were regularly distributed around the specimen circumference. Further

details about the geometry can be found in [19]. This geometry is referred to as T2 in the following. In order to characterize subsurface dwell-fatigue cracks, a third geometry was introduced to facilitate mechanical sectioning parallel to the surface. This geometry is referred to as T3 in the following. Flat dog bone specimens with a gage length of 10 mm, a gage width of 2 mm and a thickness of 1 mm were used for that purpose.

A JEOL 6100 scanning electron microscope (SEM) was employed to detect initiated cracks and to observe fracture surfaces. The local crystallographic orientations nearby the cracks were characterized using the same microscope which is equipped with an EBSD detector provided by EDAX. A step below 1.5 μm was chosen to accurately describe the local crystallographic orientations. EBSD data were processed using the OIM analysis software. Cross-section views were obtained via focused ion beam milling using a FEI Helios Nanolab G3 CX.

The cumulated plastic strain versus the number of cycles for fatigue and dwell-fatigue tests is shown in figure 1a. The mean cumulated plastic strain at failure is 9% and the average number of cycles to failure is about 3700 for dwell-fatigue tests carried out up to complete fracture (i.e. T1 specimens). For the fatigue tests, the mean plastic strain at failure is 3.6% and the average number of cycles to failure is about 10800. Thus, failure of dwell-fatigue tested specimens occurred at a higher cumulated plastic strain and a lower number of cycles, indicating a substantial dwell debit with the present testing conditions. The number of cycles to failure is reduced by a factor 2.9 with the increased load hold duration.

Figure 1 a. Cumulated plastic strain as a function of the number of cycles. Black and grey curves show a higher cumulated plastic stain and a lower number of cycles to failure for the dwell-fatigue tests. For T2 and T3 specimens, only plastic strain accumulation before test interruption is reported. b. Fracture surfaces of specimens tested up to failure showing surface crack initiation for fatigue loadings and subsurface crack initiation for dwell-fatigue loadings

SEM micrographs showing typical fracture surfaces are presented in figure 1b for fatigue and dwell-fatigue tested specimens. For the fatigue tests, the crack leading to the failure was initiated at the surface. No such surface crack initiation site was found for the dwell-fatigue tested specimens. However, numerous facets, which occasionally form clusters, are found in the center of these specimen. This observation reveals the initiation of multiple subsurface cracks for the dwell-fatigue test condition.

In order to study surface crack initiation on the fatigue tested T2 specimen, the test was interrupted after reaching a cumulated plastic strain of 1%. It corresponds to 2447 cycles. One crack among the 46 observed is presented in figure 2a. No surface crack was found on the dwell-fatigue tested T2 specimen after reaching a similar cumulated plastic strain level, which was achieved after 105 cycles. The dwell-fatigue test was then continued up to a cumulated plastic strain of 2.5%, which corresponds to 1333 cycles. 53 surface cracks were found at this stage. An example of a crack found at 2.5% plastic strain is shown in figure 2b alongside with a micrograph showing the same region after 1% plastic strain. A dwell-fatigue test on a T3 specimen was interrupted at a cumulated plastic strain of 4% and 941 cycles to investigate subsurface crack initiation. The high cumulated plastic strain was chosen to increase the probability of meeting internal cracks with mechanical sectioning. A 300 μm thick layer was removed and 20 subsurface cracks were found. A typical example is shown in figure 2a. Due to the similar features exhibited by microstructural regions surrounding the initiated cracks for all loading conditions and specimens, they are discussed altogether in the following.

As shown in figure 2, all cracks are located within α_p grain clusters and arrested nearby the boundary with transformed β regions for any loading condition. As a limited growth of surface and subsurface cracks occurred, the identification of crack initiation sites was straightforward. Except for sub-surface dwell-fatigue cracks where slip markings have been removed by the mechanical sectioning process,

slip traces indicate slip activity in α_p grains on both sides of the cracks. The slip traces are parallel to the crack. The crystallographic orientation maps suggest that crack initiation may occur at the boundary between two α_p grains. Examination of the microstructural region shown in figure 2b where dwell-fatigue surface crack initiation occurred was carried out before and after crack nucleation. It reveals that intense slip activity is localized at the interface between two α_p grains and precedes crack formation. Thinner basal slip traces are noticed in the surrounding α_p grains. The crack plane was investigated in 3D using a cross sectional view realized by FIB milling. The sharp crack extends until a grain boundary. Its path matches the basal planes on both sides of the crack in 3D. As no boundary is visible on the cross-sectional view, cracking is likely to occur along a (0001) twist boundary, which would then be aligned with the basal plane. These features are analyzed with a statistical significance in the following.

Figure 2 a. SEM micrographs and inverse pole figure maps along the loading direction showing initiated cracks and the surrounding microstructure on the surface of the fatigue tested T2 specimen, on the surface of the dwell-fatigue tested T2 specimen and in the bulk of the T3 dwell-fatigue tested specimen at different cumulated plastic strain levels and b. Micrographs of a microstructural region where crack nucleation occurred on surface of the T2 dwell-fatigue tested specimen alongside with the inverse pole figure map along the loading direction and a cross-sectional view of the crack realized using FIB milling.

The inverse pole figure shown in figure 3a reveals that the initiation α_p grains exhibit similar orientations for any loading condition and for surface or subsurface initiation. In particular, most grains exhibit declination angles between 10° and 60°. The angle between the basal plane trace and the crack path, which is denoted as $\varkappa$ in the following, has been measured on both sides of all cracks. This angle is schematically represented in figure 3b along with the corresponding distribution frequencies. A maximum frequency is observed for values lower than 5°. The basal plane trace is thus aligned with the crack path for any loading condition and both surface and subsurface cracks. As this statement holds for subsurface crack initiation, where the observation plane is randomly set during mechanical sectioning, the crack seemingly matches the basal plane in 3D.

The crystallographic misorientation across all cracks has been characterized as well and its distribution is plotted in figure 3c. While most values are lower than 30°, the maximum frequencies are obtained in the 10°-20° range. These values are too high to result only from crack opening. This is supported by the SEM micrograph of figure 3b that shows a crack opening about 1°. Therefore, a boundary seems present at crack initiation sites. As this holds for subsurface crack initiation, where the observation plane is randomly set during mechanical sectioning, the crack seemingly matches the boundary plane in 3D. Only 10 - 15 % of cracks is found in the [0°-5°[interval, where no boundary might be present. The misorientation between the c-axis of α_p grains on both sides of the crack, which is denoted as χ in the following, was also measured. The associated distribution frequencies are shown in figure 3d. Most χ values are lower than 5°. The interface between α grains is thus a (0001) twist grain boundary. This feature is consistent with the similar basal plane traces on both sides of the cracks.

Figure 3: a. Crystallographic orientation along the loading direction of the initiation α_p grains for fatigue and dwell-fatigue loadings, Distribution frequencies of b. $\varkappa$, c. Misorientation and d. χ for all test conditions demonstrating the presence of a (0001) twist boundary with a misorientation lower than 30° and that cracks are aligned with the basal and the twist boundary planes.

Several comments can be made about the previously identified features. Interestingly, no crack was detected in grains with a declination angle lower than 10° while it could be expected according to the dwell-fatigue crack initiation model initially proposed by Evans and Bache. In contrast, the analysis of the crystallographic orientation of initiation α_p grains is consistent with the works of Uta et al. [17] and Pilchak

et al. [18]. Such orientations are associated with basal slip and lead to a combination of high normal and resolved shear stress acting onto the basal plane [19,20,22,32]. Our observations are also consistent with prior studies showing that the orientation of the crack matches the basal plane trace [19,23,24,27,28]. However, the specific role of (0001) twist boundaries had not been reported yet.

For instance, Bridier et al., who investigated fatigue crack initiation in Ti-6Al-4V with a similar microstructure, have not reported the presence of such boundary at crack initiation sites [19]. The data are presently revisited in order to clarify the potential role of (0001) twist boundaries. In that study, strain controlled fatigue tests were carried out with a frequency of 1 Hz, a strain ratio of 0 and a total strain amplitude of 0.4 %. A micrograph of a secondary crack alongside with the associated crystallographic orientation map are presented in figure 4a and 4b. The misorientation profile across the crack at the nucleation site is also shown. The 14° rotation around the c-axis confirms the presence of a (0001) twist boundary. Such boundary is thus critical for fatigue and dwell-fatigue crack nucleation under a wide range of loading conditions. Although the tests carried out in the present work involve a restricted volume and a high stress in comparison with aero-engine components, they show that fatigue and dwell-fatigue crack initiation are not necessarily related to different mechanisms. Tympel et al. and Wang et al. have reported the presence of low angle (0001) twist boundaries accommodated by dislocation networks close to crack initiation sites [33,34]. However, the underlying mechanism is still unclear. Stress concentration is unlikely as i. no difference in elastic behavior is expected on both sides of such an interface due to the transversely isotropic behavior of α titanium and ii. an effect of plastic anisotropy is also unlikely as boundaries with twist angles as low as a few degrees were noticed. Interestingly, detailed transmission electron microscopy characterization by Liu et al. suggested a presence of nanometric body centered cubic β-Ti layers on such interfaces [34], which may allow the intense and localized slip that eventually leads to crack nucleation. Further investigations are on-going.

Figure 4: a. Secondary crack initiated in Ti-6Al-4V under strain controlled fatigue testing, b. The corresponding crystallographic orientation map along the loadings direction taken from [19] and c. Misorientation profile with respect to the origin along the I path of figure 4a showing the presence of a (0001) twist boundary at the crack initiation site

In summary, crack initiation was investigated in Ti-6Al-4V with a bi-modal microstructure submitted to fatigue and dwell fatigue loadings. The material was found dwell sensitive with a substantial life debit for the applied test conditions. Surface and sub-surface crack nucleation sites exhibit similar features for both fatigue and dwell-fatigue loadings. This finding suggests a common crack nucleation mechanism with the following characteristics:

- The critical microstructural configuration for fatigue and dwell fatigue crack initiation is a α_p grain pair separated by a (0001) twist boundary. The associated misorientation is most frequently in the 10° - 20° range and the boundary plane corresponds to the basal planes.
- Both α grains exhibit a declination angle in the 10°-60° range, which favors basal slip activity and a high normal stress.
- Intense and localized plasticity occurs at the (0001) twist boundary before crack nucleation.
- The crack formation proceeds along the basal plane / the twist boundary.

Acknowledgement

The Poitou-Charentes region is gratefully acknowledged for funding. This work was partially funded by the French Government programs "Investissements d'Avenir" LABEX INTERACTIFS (reference ANR-11-LABX-0017-01)

References

[1] G.Lütjering, J.C. Williams, Titanium, second ed., Springer, Berlin; NewYork, 2007.

[2] D. Eylon, J.A. Hall, Metall. Mater. Trans. A 8 (1977) 981–990.

[3] W.J. Evans, C.R. Gostelow, Metall. Mater. Trans. A 10 (1979) 1837–1846.

[4] D.L. Davidson, D. Eylon, Metall. Mater. Trans. A 11 (1980) 837–843.

[5] M.R. Bache, W.J. Evans, H.M. Davies, J. Mater. Sci. 32 (1997) 3435–3442.

[6] M.R. Bache, M. Cope, H.M. Davies, W.J. Evans, G. Harrison, Int. J. Fatigue 19 (1997) 83–88.

[7] W.J. Evans, M.R. Bache, Int. J. Fatigue 16 (1994) 443–452.

[8] F.P.E. Dunne, D. Rugg, A. Walker, Int. J. Plasticity 23 (2007) 1061–1083.

[9] V. Hasija, S. Ghosh, M.J. Mills, D.S. Joseph, Acta Mater. 51 (2003) 4533–4549.

[10] G. Venkatramani, S. Ghosh, M. Mills, Acta Mater. 55 (2007) 3971–3986.

[11] Z. Zheng, D.S. Balint, F.P.E. Dunne, Int. J. Plasticity 87 (2016) 15–31.

[12] F.P.E. Dunne, D. Rugg, Fatigue Fract. Eng. M. 31 (2008) 949–958.

[13] M.A. Cuddihy, A. Stapleton, S. Williams, F.P.E. Dunne, Int. J. Fatigue 97 (2017) 177–189.

[14] M. Anahid, M.K. Samal, S. Ghosh, J. Mech. Phys. Solids 59 (2011) 2157–2176.

[15] V. Sinha, M.J. Mills, J.C. Williams, Metall. Mater. Trans. A 37 (2006) 2015–2026.

[16] V. Sinha, M.J. Mills, J.C. Williams, J.E. Spowart, Metall. Mater. Trans. A 37 (2006) 1507–1518.

[17] E. Uta, N. Gey, P. Bocher, M. Humbert, J. Gilgert, J. Microsc. 233 (2009) 451–459.

[18] A.L. Pilchak, J.C. Williams, Metall. Mater. Trans. A 42 (2011) 1000–1027.

[19] F. Bridier, P. Villechaise, J. Mendez, Acta Mater. 56 (2008) 3951–3962.

[20] F. Bridier, P. Villechaise, J. Mendez, Acta Mater. 53 (2005) 555–567.

[21] S. Hémery, V.T. Dang, L. Signor, P. Villechaise, Metall. Mater. Trans. A (2018) 1–9.

[22] C. Lavogiez, S. Hémery, P. Villechaise, Int. J. Fatigue (2019) 105341.

[23] S.G. Ivanova, R.R. Biederman, R.D. Sisson, J. Mater. Eng. Perform. 11 (2002) 226–231.

[24] I. Bantounas, D. Dye, T.C. Lindley, Acta Mater. 57 (2009) 3584–3595.

[25] G.Q. Wu, C.L. Shi, W. Sha, A.X. Sha, H.R. Jiang, Mater. Des. 46 (2013) 668–674.

[26] S.K. Jha, C.J. Szczepanski, R. John, J.M. Larsen, Acta Mater. 82 (2015) 378–395.

[27] S.K. Jha, C.J. Szczepanski, P.J. Golden, W.J. Porter, R. John, Int. J. Fatigue 42 (2012) 248–257.

[28] K.L. Biavant, S. Pommier, C. Prioul, Fatigue Fract. Eng. M. 25 (2002) 527–545.

[29] X. Demulsant, J. Mendez, Fatigue Fract. Eng. M. 18 (1995) 1483-1497.

[30] J. Everaerts, B. Verlinden, M. Wevers, J. Microsc. 267 (2017) 57–69.

[31] J.M. Larsen, S.K. Jha, C.J. Szczepanski, M.J. Caton, R. John, A.H. Rosenberger, D.J. Buchanan, P.J. Golden, J.R. Jira, Int. J. Fatigue 57 (2013) 103–112.

[32] S. Hémery, A. Naït-Ali, M. Guéguen, J. Wendorf, A.T. Polonsky, M.P. Echlin, J.C. Stinville, T.M. Pollock, P. Villechaise, Acta Mater. 181 (2019) 36–48.

[33] P.O. Tympel, T.C. Lindley, E.A. Saunders, M. Dixon, D. Dye, Acta Mater. 103 (2016) 77–88.

[34] Y. Liu, P. Samimi, I. Ghamarian, D.A. Brice, D.E. Huber, Z. Wang, V. Dixit, S. Koduri, H.L. Fraser, P.C. Collins, JOM 67 (2015) 164–178.

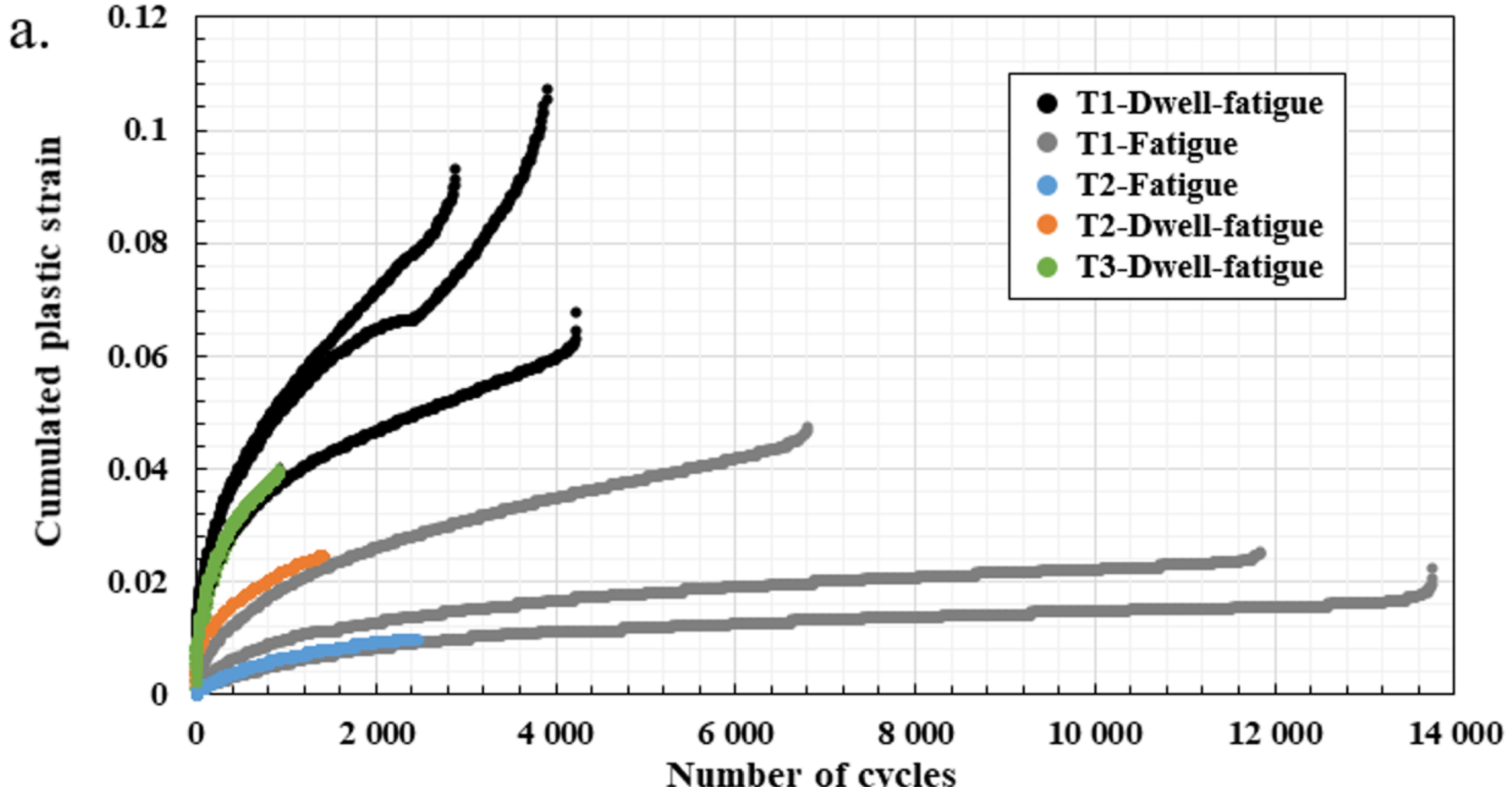
a.
0.12
0.1
0.08
0.06
0.04
0.02
0
Cumulated plastic strain
T1-Dwell-fatigue
T1-Fatigue
T2-Fatigue
T2-Dwell-fatigue
T3-Dwell-fatigue
0
2 000
4 000
6 000
8 000
10 000
12 000
14 000
Number of cycles

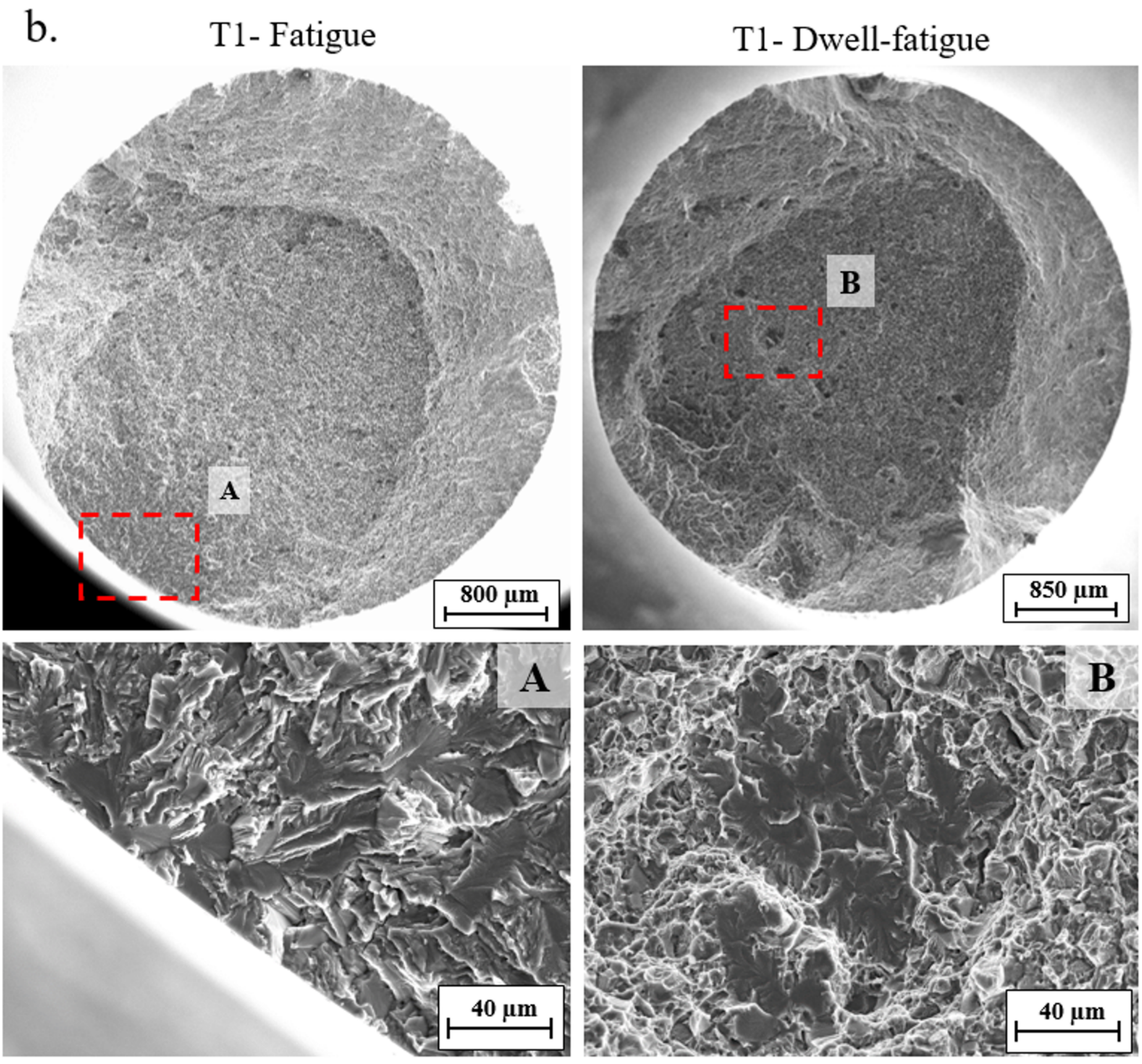
b.
T1- Fatigue
T1- Dwell-fatigue
A
B
800 µm
850 µm
A
B
40 µm
40 µm

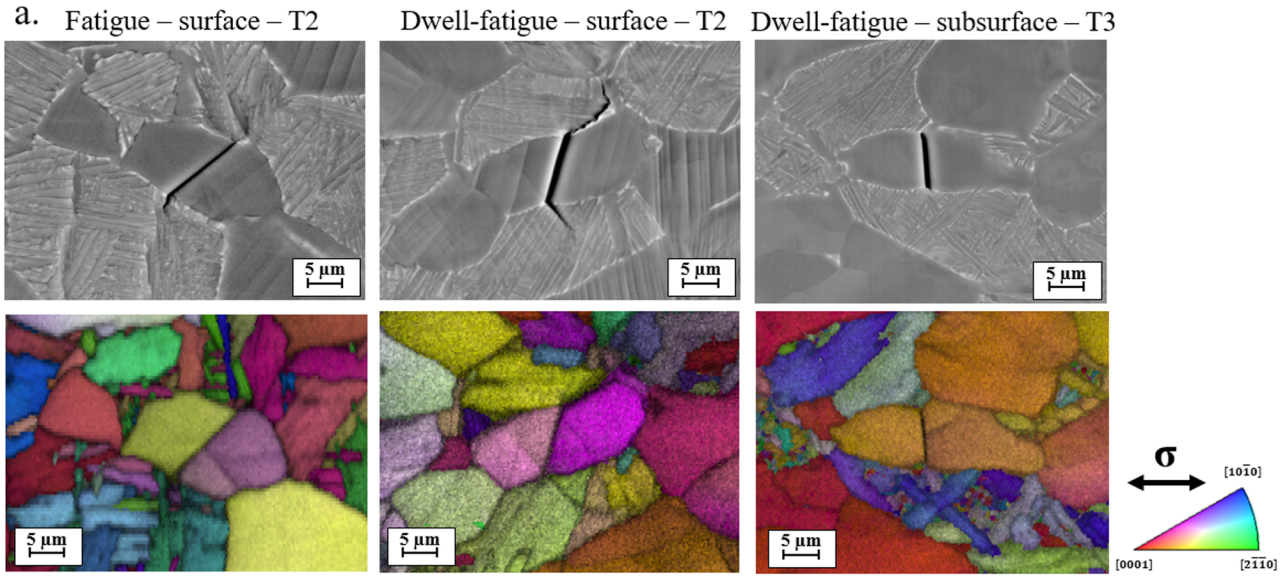
a.
Fatigue – surface – T2
Dwell-fatigue – surface – T2
Dwell-fatigue – subsurface – T3
5 µm
5 µm
5 µm
5 µm
5 µm
5 µm
σ
[10$\bar{1}$0]
[0001]
[2$\bar{1}\bar{1}$0]

b.

Dwell-fatigue – surface – T2

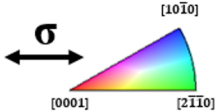

ε_p = 1% ; N_{cycles} = 105

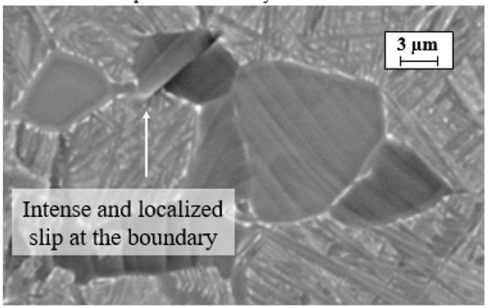

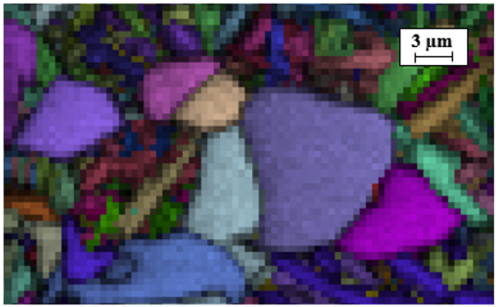

ε_p = 2,5% ; N_{cycles} = 1438

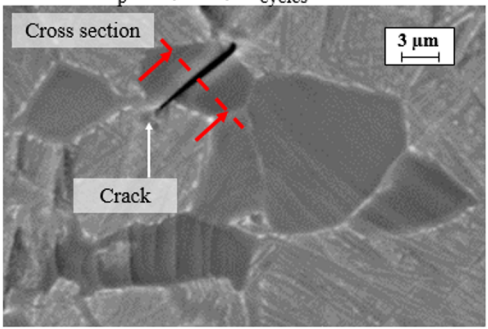

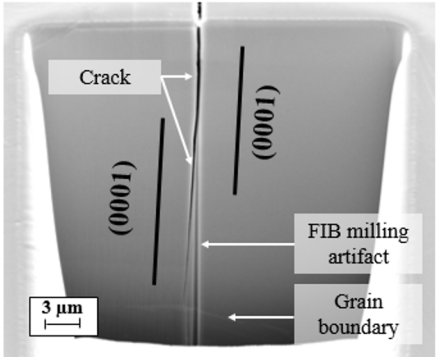

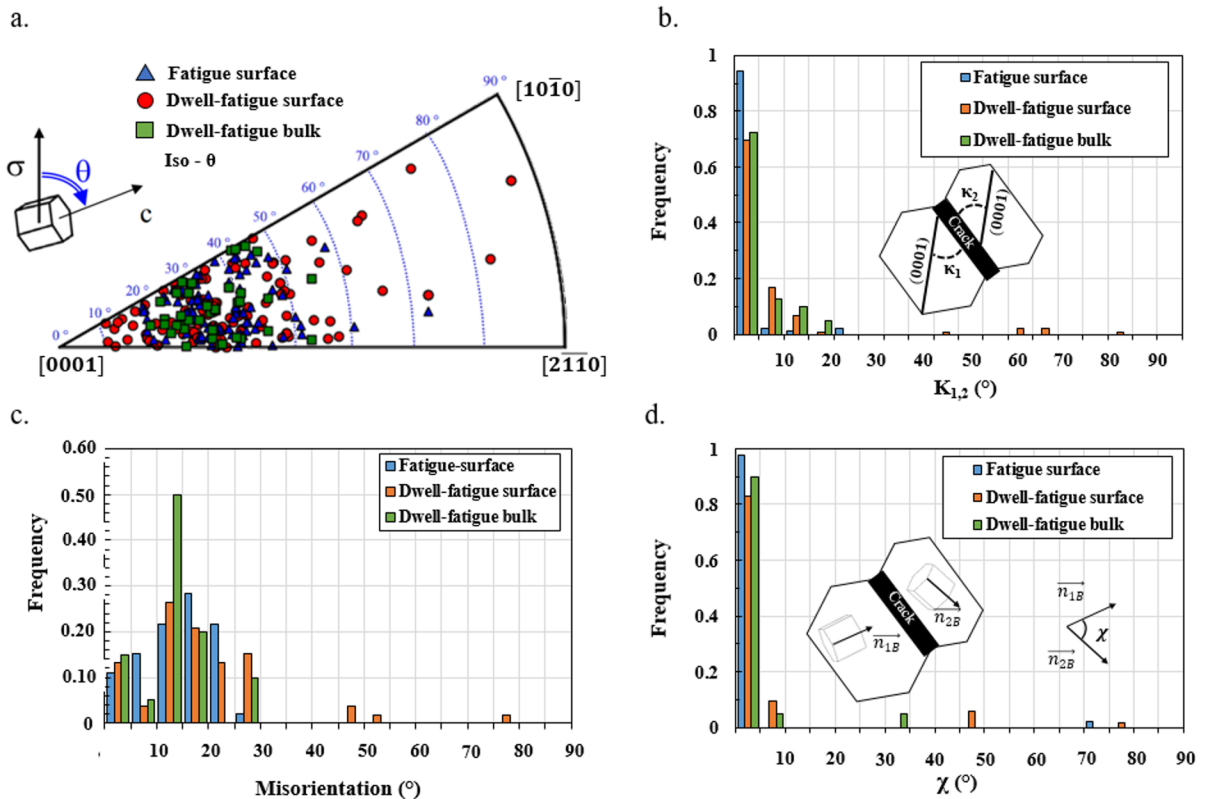
a.
Fatigue surface
Dwell-fatigue surface
Dwell-fatigue bulk
Iso - θ
σ
θ
c
90 °
80 °
70 °
60 °
50 °
40 °
30 °
20 °
10 °
0 °
[10$\bar{1}$0]
[0001]
[2$\bar{1}$10]
b.
Fatigue surface
Dwell-fatigue surface
Dwell-fatigue bulk
Frequency
Crack
(0001)
(0001)
κ_2
κ_1
$K_{1,2}$ (°)
c.
Fatigue-surface
Dwell-fatigue surface
Dwell-fatigue bulk
Frequency
Misorientation (°)
d.
Fatigue surface
Dwell-fatigue surface
Dwell-fatigue bulk
Frequency
Crack
$\vec{n}_{1B}$
$\vec{n}_{2B}$
χ
χ (°)

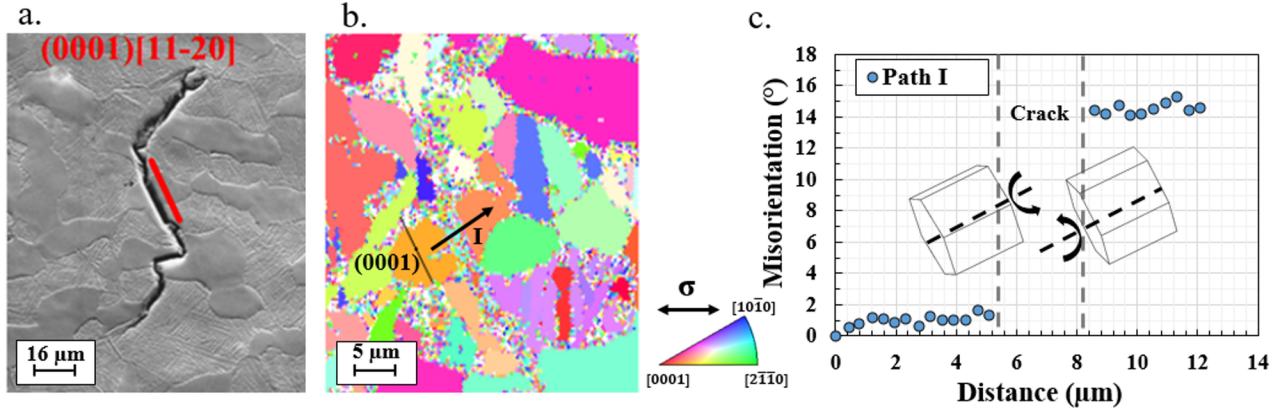
a.
(0001)[11-20]
16 μm
b.
(0001)
I
5 μm
σ
[10$\bar{1}$0]
[0001]
[2$\bar{1}\bar{1}$0]
c.
Path I
Crack
Misorientation (°)
Distance (μm)
0
2
4
6
8
10
12
14
16
18

Fatigue and dwell-fatigue crack formation at (0001) twist boundaries

After 105 dwell-fatigue cycles and $\varepsilon_p = 1\%$:

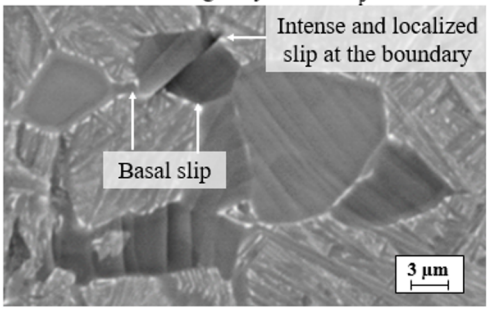

After 1438 dwell-fatigue cycles and $\varepsilon_p = 2{,}5\%$: